Hierarchical Drug Release Designed Au @PDA-PEG-MTX NPs for Targeted Delivery to Breast Cancer with Combined Photothermal-chemotherapy

Wen Li
Beijing University of Chinese Medicine
Zhiwen Cao
Beijing University of Chinese Medicine
Liuchunyang Yu
Beijing University of Chinese Medicine
Qingcai Huang
Beijing University of Chinese Medicine
Dongjie Zhu
Beijing University of Chinese Medicine
Cheng Lu
China Academy of Chinese Medical Sciences
Aiping Lu
Hong Kong Baptist University
Yuanyan Liu (yyliu_1980@163.com)
Beijing University of Chinese Medicine https://orcid.org/0000-0003-3840-5292

Research

Keywords: Au @PDA-PEG-MTX NPs, Targeted for Breast cancer, Fluorescence imaging, Hierarchical Drug Release, Combined photothermal-chemotherapy

Posted Date: January 27th, 2021

DOI: https://doi.org/10.21203/rs.3.rs-152625/v1

Abstract

Breast cancer (BC) is the frequently diagnosed cancer and one of the deadliest causes of cancer-related death with a severe survival rate. Methotrexate (MTX) is an anti-tumor drug used in the treatment of BC. The poor dispersion in water and toxic side effects limit its clinical application. Gold nanoparticles (AuNPs), due to their specific structures and unique biological and physiochemical properties, have emerged as attractive candidates as vehicles for tumor targeting, bio-imaging and therapy. An innovative nano drug-loading system (Au @PDA-PEG-MTX NPs) was prepared for targeted treatment of BC. Au @PDA-PEG-MTX NPs under near infra-red region (NIR) irradiation showed effective photothermal therapy against MDA-MB-231 human BC cells growth in vitro by inducing apoptosis through triggering reactive oxygen species (ROS) overproduction and generating excessive heat. In vivo studies revealed that Au @PDA-PEG-MTX NPs under NIR irradiation showed deep penetration and cancer-targeted fluorescence imaging application and strong photothermal therapy against BC xenograft growth in vivo by induction of apoptosis. Analysis of histopathology, cellular uptake, cytotoxicity assay, apoptosis experiment indicated that Au @PDA-PEG-MTX NPs had a good therapeutic effect with high biocompatibility and less side effect. This Au NPs drug-loading system achieved specific BC targeting ability by surface decoration of MTX, NIR laser irradiation for fluorescence imaging and combined photothermal-chemotherapy as well as pH- and NIR- triggered hierarchical drug release.

Introduction

Breast cancer (BC) is one of the most frequently observed malignant diseases among women with high mortality and economic burden[1, 2]. On account of its complicated etiology, poor response and severity side-effect to chemotherapy, both safe and efficacious are considered as the central challenge associated deaths[3]. The main aim in the fight against BC is developing effective therapeutic plans with low toxicity and high specificity to eliminate tumors[4]. However, presently used BC treatment approaches, such as surgery, chemotherapy and radiotherapy, cause diverse side effects to patients and these measures alone do not seem to achieve this aim[5]. The combination of chemotherapy drugs and the gold nanoparticles (AuNPs) drug carrier system with photothermal property can provide a promising platform for intracellular delivery of various anti-BC drugs and synergistic therapy[6, 7].

NPs designed for cancer treatment targeting can deliver chemotherapeutic drugs to specific cancer cells while reducing the exposure of normal healthy cells, so that larger doses of drugs can be delivered to the tumor site to achieve high-targeting and low-toxicity therapeutic effects.[8]. AuNPs are one type of inorganic cargo with versatile surfaces for multi-functionalization and high surface area-to-volume ratio for drug loading and superior optical properties for bioimaging and even photothermal properties for therapy, but toxicity and low biocompatibility of AuNPs are still challenges that cannot be ignored[9]. When adjusted to an appropriate size and shape, such as 15 nm size of the AuNPs have longer plasma circulation time [10, 11], the small-sized of which can be used to reduce the toxicity of AuNPs itself as an inorganic material.

Increasingly, AuNPs have attracted great attention during the past decade due to their facile synthesis and surface functionalization[12], which revealed high-performance of photothermal conversion capacity in the near infra-red region (NIR) area without harmful side effects in biological systems[13-15]. AuNPs have the characteristics of tumor NIR imaging and good stability[16]. In addition, the photothermal effect also produces excessive heat and reactive oxygen species (ROS) that destroys cancer cells[17]. To make AuNPs into perfect drug carriers, modification should be performed for targeted delivery and controlled release[18]. The strong adhesion of polydopamine (PDA) is conducive to its deposition in AuNPs, which can improve the drug loading and endow biocompatibility and the ability of AuNPs to enter mammalian cells[19]. Moreover, PDA shell can prevent the leakage of loading drugs during delivery, while achieve an on-demand drug release in the targeted location, such as NIR stimuli responsive drug release under high temperature or acidic conditions[19-21]. PEG can also improve the ability of cells to take up gold nanocomposite and prolong the cycle times in plasma [22-24]. In addition, drugs linked to PEG will be released under acidic conditions, which can lay the foundation for hierarchical drug release system[25].

Methotrexate (MTX), a folic acid analog is a highly potent antagonist on folate pathway to induce cell apoptosis, who is widely used for the treatment of rheumatoid arthritis and acute leukemia [26]. Due to its special characteristic, many experimental researches tend to explore its treatment for cancer[27]. MTX as a folic acid analog can inhibit dihydrofolate reductase (DHFR), an enzyme that helps produce tetrahydrofolate and its by-products, both of which are essential for the growth of tumor cells[28, 29]. Folate receptor (FR) is a glycosyl phosphatidylinositol (GPI)-linked protein has low expression in normal tissues, but is over-expressed in certain malignant cells such as BC[30]. Except for therapeutic purpose, as a folate analog, MTX exhibits high affinity to FR that can be targeted to deliver to BC cells. However, alike to most conventional chemotherapy drugs, the main challenge of single-agent chemotherapy is the accumulated toxicity in the body accompanied with low specificity and poor therapeutic efficacy[31]. Therefore, in recent years, the combination of chemo-therapeutics and nano-materials against BC has become an important therapeutic regimen [32]. Here, equipped MTX with AuNPs are not only as a combined photothermal-chemotherapeutic drug, but can be precisely identified as targeted ligand by whom are highly expressed on the BC surface.

In this study, Au @PDA-PEG-MTX NPs were designed for targeted delivery and hierarchical release in combination of photothermal and chemotherapy on BC with improved efficiency and low toxicity. In this innovative nano-drug loading system, AuNPs not just play roles as a drug carrier, even when modified with PDA and PEG exhibit synergistic photothermal therapeutic efficacy, bioimaging and hierarchical release stimulated with NIR and acidic conditions.

Methods

Reagents. The following chemicals were obtained from commercial sources and were used without further purification: Chloroauric acid,99.95%, from Innochem. Dopamine hydrochloride,1-ethyl-3-(3-dimethylaminopropyl) carbodiimide hydrochloride (EDCI), N-hydroxy succinimide (NHS) and Dimethyl sulfoxide (DMSO) were purchased from Sigma-Aldrich, USA. All aqueous solutions used in experiments

were deionized water (18.2 MΩ.cm) obtained from a Milli-Q water purification system. Fetal bovine serum (FBS) and DMEM/HIGH Glucose medium were purchased from Gibco, United States origin. Penicillin-Streptomycin (penicillin 100 U/ml, and streptomycin 100 mg/ml) were obtained from BI. Human breast cancer MDA-MB-231 cells were obtained from BNCC. All the antibodies were purchased from the Abcam.

Preparation of Au @PDA-PEG-MTX NPs

Preparation of AuNPs

AuNPs (15 nm in diameter) were synthesized according to the trisodium citrate reduction method reported by Frens[33]. Before all reactions started, the reaction vessel was thoroughly washed with freshly prepared aqua regia (HNO_3 / HCl = 1:3) and washed with double distilled water 3 times. First add 1 mL of 1% chloroauric acid solution to 100 mL of ultrapure water, and quickly boil it. Add 4 mL of 1% sodium citrate solution immediately. When the color of the solution changes from light yellow to wine red, gold nanoparticles AuNP with an average diameter of 15 nm will be formed and stored under dark conditions at 4°C. The average size of AuNP was estimated by transmission electron microscope (TEM, HT7700, Tokyo, Japan, Hitachi).

Preparation of Au @PDA NPs Bioconjugates

Disperse the previously synthesized AuNPs in 50 mL pH 8.5 Tris-HCl buffer, and the solution concentration is 2 mg/mL at this time. In the dark, this solution is subjected to strong magnetic stirring overnight after 5mL (2mg/mL) of the prepared dopamine solution added dropwise to the solution. A black solution is obtained, which is centrifuged at 12,000 rpm at 4°C for 10 minutes; the supernatant is discarded, and the black precipitate is collected, and washed with deionized water repeatedly for 3 times.

Preparation of Au @PDA-PEG NPs

Disperse the synthesized Au @PDA NPs complex in 50 mL of deionized water. At this time, the concentration of the dispersion solution was 2 mg/ml. In the dark, added NH2-PEG-SH (2k) (2 mg/mL) dropwise to the solution and stirred it magnetically overnight. Then, it was centrifuged at 12,000 rpm at 4°C for 10 minutes to obtain Au @PDA-PEG NP, which was washed repeatedly with deionized water for 3 times[34].

Preparation of Au @PDA-PEG-MTX NPs

In order to modify the folate receptor targeting drug MTX on the synthesized Au @PDA-PEG NPs, 8 mg MTX, 4 mg EDCI and 2.8 mg NHS were added to 50 mL of Au @PDA-PEG NPs aqueous solution under magnetic stirring. After 3 hours of magnetic stirring in the dark, centrifuge at high speed at 4°C (12,000 rpm, 10 min), save the supernatant, and wash the precipitate with deionized water 3 times. The precipitate was Au @PDA-PEG-MTX NPs bioconjugate.

Preparation of Au @PDA/FITC-PEG-MTX NPs

The synthesized Au @PDA-PEG-MTX NPs bioconjugate was re-dispersed in 2 mL deionized water (2 mg/mL). In the dark state, magnetically stir continuously for 12 hours at room temperature, and add 50 µl of DMSO solution containing 10% (w/w) FITC fluorescent agent. The resulting mixture solution was then centrifuged at 4°C (12,000 rpm, 10 minutes), and the precipitate obtained after centrifugation was washed with deionized water three times. The final product was Au @PDA / FITC-PEG-MTX NPs.

Drug loading study of Au @PDA-PEG-MTX NPs

For MTX loading, UV-vis spectroscopy was used to determine the absorbance of the washed drug, the absorbance of the supernatant solution and the absorbance strength of the initial drug. The MTX loading efficiency was as follows:

$$\text{Loading efficiency (\%)} = \frac{(A_{Drug} - A_S - A_W)}{A_{Drug}} \times 100\%$$

A_W was absorbance of the drug after washing, A_S was absorbance of supernatant and A_{Drug} was absorbance intensity of initial drug[30].

In vitro MTX release pattern from Au @PDA-PEG-MTX NPs Au @ The PDA-PEG-MTX NPs bioconjugate was dissolved in 10 mL phosphate buffer solution (20 mM) with pH 5.4 and 7.4, and the solution system was placed in a ready-to-use dialysis bag with a molecular weight cut-off of 1 kda. At the same time, add protease (1 mg/ml) to the phosphate buffer to cleave the amide bond between MTX and PEG[35]. At the specified time point, 500µl of the dialyzed solution was collected to obtain the released MTX, and the absorbance was measured at 305 nm by ultraviolet-visible spectroscopy (UV-vis, PerkinElmer, Singapore) [36].

Characterization of Au @PDA-PEG-MTX NPs and its intermediate products

A UV-Vis spectrometer was used to record the UV-Vis absorption spectrum of the synthesized gold nanoparticles (15nm). A vacuum Fourier transform infrared spectrometer (FT-IR, America, Thermo Fisher Scientific) was used to record the Fourier transform infrared spectrum of MTX-PEG. The morphology of AuNPs, Au @PDA NPs and Au @PDA-PEG-MTX NPs were recorded by TEM. The Brookhaven Zeta PALS instrument was used to record the dynamic light scattering (DLS) and zeta potential of AuNPs, Au @PDA NPs, Au @PDA-PEG NPs and Au @PDA-PEG-MTX NPs.

Biological experiments

Cell culture and in vitro cytotoxicity assay

The human BC MDA-MB-231 cells were cultured in a high glucose medium containing 10% FBS, and the parameters of the incubator were set to 37°C and 5% CO_2[37]. The MDA-MB-231 cells were digested with trypsin containing EDTA, and the MDA-MB-231 cells were digested and seeded on a transparent 96-well

plate. The cell density of each well was 1.8×105 cells. Incubate overnight in an incubator to allow cells to attach to 96-well plates. After adding 2.5-30 μg/mL Au @PDA-PEG-MTX NPs for 12 h, the cells were treated with or without 808 nm NIR irradiation (200mW/cm2) for a total of 20 minutes. CCK-8 was added to measure and evaluate cell viability. Use a microplate reader (Tecan M200 PRO) to measure absorbance at 450nm wavelength. The cell survival rate (%) was calculated as (average absorbance value of the treatment group/average absorbance value of the control group) ×100%. Repeat the measurement 3 times.

In vitro cellular uptake ofAu @PDA-PEG-MTX NPs

The uptake of Au @PDA / FITC-PEG-MTX NPs by MDA-MB-231 cells was recorded by a confocal laser scanning microscope. Digest the cells with trypsin, inoculate 1 ml of MDA-MB-231 cells (1×10^5) into a glass-bottom cell culture dish, and incubate in an incubator for 24 h. Remove the original medium and wash the cells with PBS. Use nanocomposite Au @PDA/FITC-PEG-MTX with a concentration of 15μg/ml, 20μg/ml, 25μg/ml to replace this medium. Incubate in an incubator for 4 hours to fully absorb the drug. Wash the cells with PBS three times and fix them with 4% cell fixation solution (1 ml/well) at 4°C for 30 minutes. The cells were washed 3 times with PBS, and then stained with DAPI solution (2 ml/well) for 5 min to ensure coloration of the nuclei. After washing the cells with PBS, confocal laser scanning imaging was performed.

Measurement of ROS generation

MDA-MB-231 cells were seeded in 6-well plates (10^5 cells/well) and divided into 3 groups of blank cells, Au @PDA-PEG-MTX NPs and NIR + Au @PDA-PEG NPs. Incubate for 24 hours in a cell culture incubator. The NIR + Au @PDA-PEG NPs group used 808nm NIR laser radiation to treat the cells. The DCFH-DA probe was diluted 1:1000 in serum-free medium, and the medium containing the DCFH-DA probe was added to each well to cover the cells, and then incubated in an incubator for 30 minutes. Then, wash the cells with PBS and use a laser confocal microscope to set the excitation wavelength to 488nm and the emission wavelength to 525nm to check the generation of ROS.

Western blot analysis

The cells were treated with MTX, Au @PDA-PEG-MTX NPs and NIR+Au @PDA-PEG-MTX NPs and protein was extracted, and the total protein was quantified using the BCA kit. Western blotting was used to analyze the effects of MTX, Au @PDA-PEG-MTX NPs and NIR+Au @PDA-PEG-MTX NPs on the expression of Bcl-2, Bax, Caspase 7 and Caspase 9 proteins involved in the apoptotic pathway.

In vivo biodistribution

BALB/c female nude mice were administered intravenous tail injections with Au @PDA-PEG-MTX NPs. The fluorescence images of the nude mice were detected at 0, 2, 6, 12, 24 and 48 h after injection using the IVIS Spectrum in vivo fluorescence imaging system.

In vivo anticancer effects

BALB/c female nude mice were purchased from Beijing Vital River Laboratory Animal Technology Co., Ltd. and bred in a sterile environment (SPF). The tumor model was established by subcutaneously injecting MDA-MB-231 cells (10^6 cells in 100 μL) into the armpit of nude mice. After 16 days of inoculation, the tumor volume reached 90mm3. The mice were randomly divided into four groups, each with 6 mice, namely the saline control group, the MTX treatment group, the Au @PDA-PEG-MTX NPs treatment group and the NIR+Au @PDA-PEG-MTX NPs treatment group. The mice were administered by intravenous tail injection, and the weight of the mice was recorded in real time. After 19 days of treatment, the mice were sacrificed and th**e** tumor mass was surgically removed to measure the volume and weighed. The tumor inhibitory rate was as follows:

$$\text{Tumor inhibitory rate (\%)} = \frac{W_c - W_o}{W_c} \times 100\%$$

W_c was the average tumor weight of the control group, W_o was the average tumor weight of average tumor weight of operation group.

Safety evaluation of Au @PDA-PEG-MTXNPs

In order to evaluate the toxicity of Au @PDA-PEG-MTX NP and NIR+Au @PDA-PEG-MTX NP during in vivo treatment, healthy ICR mice were set as the control group, and ICR mice were sacrificed 30 days after administration. The important organs of mice (liver, spleen, kidney, heart and lung) were collected and stained with H&E to observe histopathological changes.

Statistical analysis

All data and images were from three independent experiments. Data were expressed as mean ± SD. Statistical analysis was performed by Prism graph pad 8.0, and then Tukey's post-test was performed. *P<0.05 vs. blank, **P<0.01 vs. blank.

Results And Discussion

Characterization of Au @PDA-PEG-MTX NPs and its intermediate products

In the TEM (Figure 3), the uniform size of AuNPs prepared by sodium citrate reduction method was observed, and the diameter was about 15 nm. Dopamine polymerized spontaneously in an alkaline environment and adsorbed on the surface of AuNPs to form polydopamine. The shape of Au @PDA NPs was shown in Figure 3. In order to improve the dispersibility and biocompatibility of AuNPs in aqueous solutions, NH2-PEG-SH (2k) was introduced, which successfully connected with Au @PDA NPs through the Michael addition reaction between sulfhydryl groups and PDA. Finally, the targeted drug MTX was connected to Au @PDA-PEG NPs through the condensation reaction of the carboxyl group and the amino

group of NH2-PEG(2k)-SH to form an amide bond. AuNPs, Au @PDA NPs, Au @PDA-PEG NPs, Au @PDA-PEG-MTX NPs all showed excellent dispersibility in solution, as shown in Figure 2D for the measurement results of dynamic light scattering (DLS). The final particle size of the synthesized Au @PDA-PEG-MTX NPs was about 150nm. From Au NP to Au @PDA-PEG-MTX NP, the zeta potential of each step in the synthesis process changed, indicating that the modification was successfully carried out in each step of the process (Figure 2C).

AuNPs were one of the commonly used inorganic nanocarriers. Under the irradiation of near infrared light, they would generate heat and reactive oxygen to promote cell apoptosis.15nm-sized gold nanoparticles were experimentally proven to be less toxic than other-sized nanoparticles, which owed better tissue penetration and would not be recognized and cleared in the blood circulation [23]. PDA had low toxicity and was easily soluble in water, which could improve the toxicity and biocompatibility of the gold nanocomposite. In addition, PDA absorbed in the near-infrared light region, and would disintegrate itself under high temperature or acidic conditions to cause drug release, becoming a potential photothermal therapeutic. Experiments had proved that PEG can be used to functionalize Au and modify the surface of Au to facilitate further drug loading and reduce toxicity. Moreover, PEG could improve the ability of cells to take up gold nanocomposite. MTX as a commonly used anti-BC drug causes certain toxicity to normal tissues in the process of metabolism due to the production of various metabolites, which was also a tumor targeting ligand. The Au @PDA-PEG-MTX NPs could have good biocompatibility, dispersion and tumor targeting.

Drug loading and release

The MTX loading efficiency was determined by comparing the absorbance of the supernatant obtained by centrifuging the drug-loaded particles with the absorbance of the initial drug in the drug-loading experiment. MTX was an anti-BC drug with strong side effects. In this study, the carboxyl group of MTX was coupled with amine functionalized polyethylene glycol to reduce toxicity and improve the effect of anti-BC. The data showed that when the ratio of drug to particles was 3:1, the loading efficiency of MTX was 36.21%.

In order to evaluate the MTX release ability of Au @PDA-PEG-MTX NP in the normal physiological (pH 7.4) environment and tumor lysosomal (pH 5.5) microenvironment in the body, UV spectrophotometry was used to determine the MTX release capacity at pH 7.4 and pH 5.5. PBS buffer was used as a simulated body fluid. Figure 4 showed the release of MTX at pH 5.4 and pH 7.4 after 48 hours. The release of MTX from Au @PDA-PEG-MTX NPs was pH-dependent. At pH 5.5, MTX was released rapidly, with a cumulative release of 64.83% within 48 hours. This release might be attributable to the hydrolysis of the amide bond connected to MTX to release a large amount of drug under the acidic conditions of the simulated lysosome. At pH 7.4 the release of MTX after 48 hours was 28.97%, and a small amount of MTX release was probably due to the fact that the amide bond was relatively stable under normal physiological conditions. In addition, the release of MTX from Au @PDA-PEG-MTX NPs treated with NIR laser irradiation was also studied. Using 808nm NIR laser to irradiate Au @PDA-PEG-MTX NPs solution,

the release percentage of MTX reached 81.56% after 48 hours, which was much higher than the release of MTX without NIR laser irradiation under the same conditions (64.83%). We speculated that in addition to being bonded to the gold nanocomposite by means of amide bonds, MTX could also be adsorbed on the surface of the gold nanocomposite through its adhesion to dopamine.

Cellular uptake of Au @PDA-PEG-MTX NPs

The degree to which the nanomedicine was taken up by the cells would affect the delivery and therapeutic effect of the drug. In order to facilitate the observation of the uptake of the synthesized nanocomposite in the cell, Au @PDA-PEG-MTX NP was labeled with FITC. After MDA-MB-231 cells were incubated with Au @ PDA / FITC-PEG-MTX NPs, confocal laser scanning imaging showed strong fluorescence signals of Au @ PDA / FITC-PEG-MTX NPs in the cytoplasm.

The result suggested that the Au @PDA-PEG-MTX NPs can be efficiently internalized by the human BC MDA-MB-231 cells. In addition, the result also showed that under different dosages, different fluorescence intensities represented different cell uptake capabilities. The results showed that the drug had the strongest fluorescence intensity at 25μg/ml, indicating that the drug at this concentration had a strong cell uptake ability. (Figure 6)

ROS detection in MDA-MB-231 cells

Photothermal therapy could cause the production of ROS. In recent years, studies on ROS had found that ROS can achieve the purpose of treatment by accelerating tumor cell death, which was considered to be the main anti-cancer mechanism of photothermal therapy. Therefore, a laser confocal microscope was used to detect the generation of ROS in cells treated with NIR+Au @PDA-PEG-MTX NPs.

As shown in Figure 7, the green fluorescence of Au @PDA-PEG-MTX NPs under NIR treatment was enhanced compared to the blank cells in the control group and Au @PDA-PEG-MTX NPs. It shows that Au @PDA-PEG-MTX NPs under NIR treatment will generate more ROS. The results showed that Au @PDA-PEG-MTX NPs under NIR irradiation caused overproduction of ROS.

The expression of apoptotic-related proteins in MDA-MB-231 Cells Apoptosis referred to the orderly and autonomous death of cells controlled by genes in order to maintain a stable internal environment[38]. Mitochondria were the control center of cell life activities. It was not only the center of cell respiratory chain and oxidative phosphorylation, but also the center of apoptosis regulation. Caspase played an essential role in the process of apoptosis[39]. It was reported that the release of cytochrome C from mitochondria was a key step in cell apoptosis. The cytochrome C released into the cytoplasm promoted the activation of Caspase-9, and then activated Caspase-9 could activate the downstream Caspase-3, inducing cell apoptosis[40]. As shown in the Figure 8, cells treated with Au @PDA-PEG-MTX NPs with NIR laser irradiation, Au @PDA-PEG-MTX NPs alone or MTX alone showed protein expression trends. An increase in the expression of Caspase-3 and Caspase-9 were observed in MDA-MB-231 cells following

treatment with Au @PDA-PEG-MTX NPs with NIR laser irradiation group compared with group Au @PDA-PEG-MTX NPs alone or MTX alone groups.

The Bcl-2 family was the main role of anti-apoptosis. They were key regulators of mitochondrial pathways. Overexpression of anti-apoptotic Bcl-2 and decreased expression of pro-apoptotic Bax were common in many human cancers. Bax was the first member of the pro-apoptotic family discovered, and it was mainly located in the cytoplasm of normal cells. Bax was up-regulated after being stimulated by apoptosis and transferred to the mitochondria, directly or indirectly forming pores in the mitochondria, causing the release of cytochrome C. Accordingly, the expression of the anti-apoptotic protein Bcl-2 was down-regulated. As shown in the Figure 8, in the NIR+Au @PDA-PEG-MTX NPs group, compared with the Au @PDA-PEG-MTX NPs alone and the MTX alone group, the expression of Bax increased and the expression of Bcl-2 decreased.

In summary, NIR+Au @PDA-PEG-MTX NPs was a better way to treat BC.

In vivo distribution and anticancer activity

As shown in the Figure 9, after injection of Au @PDA-PEG-MTX NPs into the body through the tail vein, the mice exposed to NIR showed obvious biofluorescence in the tumor and surrounding areas. After 6 hours, the fluorescent signal was detected in the tumor area as early as possible, and the complete aggregation to the tumor site was finally completed at 12 hours, which confirmed the tumor-targeted imaging of Au @PDA-PEG-MTX NPs in vivo.

The anti-BC activity in vivo was evaluated in BALB/c nude mice bearing MDA-MB-231 cancer xenografts. The BC tumor volume of mice in the control group (normal saline) increased by about 15 times. After 19 days of treatment, the tumor weight of BC treated with MTX alone was reduced by 44.68%. The inhibition rate of BC tumors in the Au @PDA-PEG-MTX NPs group under NIR irradiation was 70.21%, which was much higher than that when MTX was used alone.

Photos of BALB/c nude mice and BC solid tumors were arranged in the Figure 10 A. The results showed that tail vein injection of MTX alone could slightly suppress the volume of BC tumors. However, after Au @PDA-PEG-MTX NPs combined with near-infrared radiation treatment, the BC tumor volume was significantly suppressed. Statistical analysis of BC tumor volume (Figure 10 B), body weight changes of mice (Figure 10 C) and BC tumor weight (Figure10 D) further confirmed this in vivo growth inhibitory effect.

Safety evaluation in vitro

Side effect of the Au @PDA-PEG-MTX NPs and NIR+Au @PDA-PEG-MTX NPs were examined to evaluate its safety. H&E staining was performed for histopathological changes. As shown in Figure 11, in the control group, cardiomyocytes were arranged neatly, with abundant cytoplasm, intact membrane and clearly visible nucleus, with no or occasional inflammatory cell infiltration. The Au @PDA-PEG-MTX NPs and NIR+Au @PDA-PEG-MTX NPs groups were similar to the control group. In the control group, the

number of hepatocytes was very abundant, the hepatic cords were neatly arranged, clear, and complete, without obvious abnormalities, the blood vessels were round, there was little inflammation around the liver, and the liver lobules were rarely inflamed. In the Au @PDA-PEG-MTX NPs group, hepatocytes were slightly swollen and deformed, hepatocytes had many fat droplets, liver lobules were degenerated, liver cords were arranged irregularly, and liver lobules were inflamed. The NIR+Au @PDA-PEG-MTX NPs group was similar to the control group. In the control group, the glomerulus volume was roughly normal, the size was relatively uniform, the glomerular basement membrane was roughly intact, the tubular epithelial cells were arranged neatly, and the tubular and interstitial-interstitial structures were acceptable. The volume and size of the glomeruli in the Au @PDA-PEG-MTX NPs group were inconsistent. The cells in the glomeruli increased more than normal, the extracellular matrix increased more than normal, and the arrangement of renal tubular epithelial cells was irregular. The structure of the renal tubules was unclear. The NIR+Au @PDA-PEG-MTX NPs group was similar to the control group. In the control group and the two experimental groups, the lung tissue structure was relatively clear, the entire alveolar structure was relatively complete, the thickness of the alveolar wall was relatively normal, and the degree of bronchial stenosis was relatively light. Alveolar epithelial cells, eosinophils and lymphocytes rarely infiltrate the alveolar cavity, and the congestion sites in the alveoli and alveolar septum were significantly reduced. In the control group, the spleen had a clear structure, red and white pulps were neatly distributed, and no sinus congestion was seen. The structure of splenic nodules was clear. The structural characteristics of the two experimental groups were similar to those of the control group.

These results indicated that the Au @ PDA-PEG-MTX NPs group and NIR+Au @ PDA-PEG-MTX NPs had similar histological characteristics compared with the control group. Except for the slight liver and kidney damage in the Au @ PDA-PEG-MTX NPs group, no significant damage or inflammation was observed in all groups.

Conclusion

A novel nanoplatform based on hierarchical drug release for chemo-photothermal treatment on BC was designed, which showed excellent antitumor efficacy and low toxicity. As a drug carrier, AuNPs show good biocompatibility, stability and drug release triggered by NIR laser irradiation/pH. When the Au @PDA-PEG-MTX NPs were taken up by tumor cells, MTX was released through amide bond cleavage in the specific acidic microenvironment (pH 5.5) of the lysosome to achieve the first step of chemotherapy. Subsequently, NIR laser irradiation caused the AuNPs to generate heat, and the MTX adsorbed on the surface of dopamine was released in a second step. The synthesized nano drug-carrying system generates heat as well as a large amount of ROS, realizing chemotherapy, photothermal and photodynamic multiple therapy to treat BC. The as-synthesized NPs promoted circulation and targeted delivery of the drug accompanied with bioimaging. We believe that the combination of multiple therapies to treat cancer is a promising strategy that will accelerate the further development of the field of oncology. In future research, detailed mechanism in the delivery process and action forms will be pursued in-depth for clinical purpose.

Declarations

Ethics approval and consent to participate

All animal experiments were conducted under the Ethical and Regulatory Guidelines for Animal Experiments defined by Institute of Basic Theory, China Academy of Chinese Medical Sciences (License Number: SCXK (Beijing) 2016-0011, SYXK (Beijing) 2017-0033).

Consent for publication

All authors agreed to submit this manuscript.

Availability of data and materials

All data generated or analyzed during this study are included in this published article.

Competing Interests

The authors have declared that no competing interest exists.

Funding

This work was supported by the National Science Foundation of China (Project No. 81573569 and 81873009) and National Science and Technology Major Project (2018ZX10101001-005-003 and 2018ZX10101-001-005-004). All special thanks for the long-term subsidy mechanism from the Ministry of Finance and the Ministry of Education of PRC for BUCM.

Authors' contributions

WL and YYL designed the project. LCYY, QCH and DJZ were involved in the discussion. CL and APL directed the experiment. WL and ZWC performed the experiments. WL analyzed the data. WL and YYL wrote the manuscript. All authors read and approved the final manuscript.

Acknowledgments

Not applicable.

Authors' information

[1]School of Chinese Materia Medica, Beijing University of Chinese Medicine, Beijing 100029, China. [2]Institute of Basic Research in Clinical Medicine, China Academy of Chinese Medical Sciences, Beijing 100700, China. [3]School of Chinese Medicine, Hong Kong Baptist University, Kowloon, Hongkong, China.

References

[1] Adak A, Unal YC, Yucel S, Vural Z, Turan FB, Yalcin-Ozuysal O, et al. Connexin 32 induces pro-tumorigenic features in MCF10A normal breast cells and MDA-MB-231 metastatic breast cancer cells. Biochimica et biophysica acta Molecular cell research 2020;1867:118851.

[2] Xiong K, Zhang Y, Wen Q, Luo J, Lu Y, Wu Z, et al. Co-delivery of paclitaxel and curcumin by biodegradable polymeric nanoparticles for breast cancer chemotherapy. International journal of pharmaceutics 2020;589:119875.

[3] Kim J, Shim M, Yang S, Moon Y, Song S, Choi J, et al. Combination of cancer-specific prodrug nanoparticle with Bcl-2 inhibitor to overcome acquired drug resistance. Journal of controlled release : official journal of the Controlled Release Society 2020.

[4] Venetis K, Invernizzi M, Sajjadi E, Curigliano G, Fusco N. Cellular immunotherapy in breast cancer: The quest for consistent biomarkers. Cancer treatment reviews 2020;90:102089.

[5] Nunnery SE, Mayer IA. Targeting the PI3K/AKT/mTOR Pathway in Hormone-Positive Breast Cancer. Drugs 2020.

[6] Tabassam Q, Mehmood T, Raza A, Ullah A, Saeed F, Anjum F. Synthesis, Characterization and Anti-Cancer Therapeutic Potential of Withanolide-A with 20nm sAuNPs Conjugates Against SKBR3 Breast Cancer Cell Line. International journal of nanomedicine 2020;15:6649-58.

[7] Zhu Y, Yang L, Xu J, Yang X, Luan P, Cui Q, et al. Discovery of the anti-angiogenesis effect of eltrombopag in breast cancer through targeting of HuR protein. Acta pharmaceutica Sinica B 2020;10:1414-25.

[8] He H, Liu L, Zhang S, Zheng M, Ma A, Chen Z, et al. Smart gold nanocages for mild heat-triggered drug release and breaking chemoresistance. Journal of controlled release : official journal of the Controlled Release Society 2020;323:387-97.

[9] Wang W, Li D, Zhang Y, Zhang W, Ma P, Wang X, et al. One-pot synthesis of hyaluronic acid-coated gold nanoparticles as SERS substrate for the determination of hyaluronidase activity. Mikrochimica acta 2020;187:604.

[10] Bhatia E, Banerjee R. Hybrid silver-gold nanoparticles suppress drug resistant polymicrobial biofilm formation and intracellular infection. Journal of materials chemistry B 2020;8:4890-8.

[11] Bai X, Wang Y, Song Z, Feng Y, Chen Y, Zhang D, et al. The Basic Properties of Gold Nanoparticles and their Applications in Tumor Diagnosis and Treatment. International journal of molecular sciences 2020;21.

[12] Chandrasekaran R, Madheswaran T, Tharmalingam N, Bose R, Park H, Ha D. Labeling and tracking cells with gold nanoparticles. Drug discovery today 2020.

[13] Wang J, Zhang Y, Jin N, Mao C, Yang M. Protein-Induced Gold Nanoparticle Assembly for Improving the Photothermal Effect in Cancer Therapy. ACS applied materials & interfaces 2019;11:11136-43.

[14] Zheng T, Wang W, Wu F, Zhang M, Shen J, Sun Y. Zwitterionic Polymer-Gated Au@TiO2 Core-Shell Nanoparticles for Imaging-Guided Combined Cancer Therapy. Theranostics 2019;9:5035-48.

[15] Hou Z, Wang Z, Liu R, Li H, Zhang Z, Su T, et al. The effect of phospho-peptide on the stability of gold nanoparticles and drug delivery. Journal of Nanobiotechnology 2019;17.

[16] Amouzadeh Tabrizi M, Shamsipur M, Saber R, Sarkar S. Isolation of HL-60 cancer cells from the human serum sample using MnO2-PEI/Ni/Au/aptamer as a novel nanomotor and electrochemical determination of thereof by aptamer/gold nanoparticles-poly(3,4-ethylene dioxythiophene) modified GC electrode. Biosensors & bioelectronics 2018;110:141-6.

[17] Malaikolundhan H, Mookkan G, Krishnamoorthi G, Matheswaran N, Alsawalha M, Veeraraghavan V, et al. Albizia lebbeckAnticarcinogenic effect of gold nanoparticles synthesized from on HCT-116 colon cancer cell lines. Artificial cells, nanomedicine, and biotechnology 2020;48:1206-13.

[18] Zheng Y, Zhang J, Zhang R, Luo Z, Wang C, Shi S. Gold nano particles synthesized from Magnolia officinalis and anticancer activity in A549 lung cancer cells. Artificial cells, nanomedicine, and biotechnology 2019;47:3101-9.

[19] Scarano S, Palladino P, Pascale E, Brittoli A, Minunni M. Colorimetric determination of p-nitrophenol by using ELISA microwells modified with an adhesive polydopamine nanofilm containing catalytically active gold nanoparticles. Mikrochimica acta 2019;186:146.

[20] Sy KHS, Ho LWC, Lau WCY, Ko H, Choi CHJ. Morphological Diversity, Protein Adsorption, and Cellular Uptake of Polydopamine-Coated Gold Nanoparticles. Langmuir : the ACS journal of surfaces and colloids 2018;34:14033-45.

[21] Cai S, Yan J, Xiong H, Xing H, Liu Y, Liu S, et al. Aptamer-Functionalized Molybdenum Disulfide Nanosheets for Tumor Cell Targeting and Lysosomal Acidic Environment/NIR Laser Responsive Drug Delivery to Realize Synergetic Chemo-Photothermal Therapeutic Effects. International journal of pharmaceutics 2020:119948.

[22] Mao W, Kim HS, Son YJ, Kim SR, Yoo HS. Doxorubicin encapsulated clicked gold nanoparticle clusters exhibiting tumor-specific disassembly for enhanced tumor localization and computerized tomographic imaging. Journal of controlled release : official journal of the Controlled Release Society 2018;269:52-62.

[23] Feito MJ, Diez-Orejas R, Cicuendez M, Casarrubios L, Rojo JM, Portoles MT. Characterization of M1 and M2 polarization phenotypes in peritoneal macrophages after treatment with graphene oxide nanosheets. Colloids and surfaces B, Biointerfaces 2019;176:96-105.

[24] Liu R, An Y, Jia W, Wang Y, Wu Y, Zhen Y, et al. Macrophage-mimic shape changeable nanomedicine retained in tumor for multimodal therapy of breast cancer. Journal of Controlled Release 2020;321:589-601.

[25] He Y, Cong C, Li X, Zhu R, Li A, Zhao S, et al. Nano-drug System Based on Hierarchical Drug Release for Deep Localized/Systematic Cascade Tumor Therapy Stimulating Antitumor Immune Responses. Theranostics 2019;9:2897-909.

[26] Murawala P, Tirmale A, Shiras A, Prasad BL. In situ synthesized BSA capped gold nanoparticles: effective carrier of anticancer drug methotrexate to MCF-7 breast cancer cells. Materials science & engineering C, Materials for biological applications 2014;34:158-67.

[27] Ong Y, Bañobre-López M, Costa Lima S, Reis S. A multifunctional nanomedicine platform for co-delivery of methotrexate and mild hyperthermia towards breast cancer therapy. Materials science & engineering C, Materials for biological applications 2020;116:111255.

[28] Ong YS, Banobre-Lopez M, Costa Lima SA, Reis S. A multifunctional nanomedicine platform for co-delivery of methotrexate and mild hyperthermia towards breast cancer therapy. Materials science & engineering C, Materials for biological applications 2020;116:111255.

[29] Ali EMM, Elashkar AA, El-Kassas HY, Salim EI. Methotrexate loaded on magnetite iron nanoparticles coated with chitosan: Biosynthesis, characterization, and impact on human breast cancer MCF-7 cell line. International journal of biological macromolecules 2018;120:1170-80.

[30] Dutta B, Nema A, Shetake NG, Gupta J, Barick KC, Lawande MA, et al. Glutamic acid-coated Fe3O4 nanoparticles for tumor-targeted imaging and therapeutics. Materials science & engineering C, Materials for biological applications 2020;112:110915.

[31] Chen TW, Jan IS, Chang DY, Lin CH, Chen IC, Chen HM, et al. Systemic treatment of breast cancer with leptomeningeal metastases using bevacizumab, etoposide and cisplatin (BEEP regimen) significantly improves overall survival. Journal of neuro-oncology 2020;148:165-72.

[32] Wang C, Vazquez-Gonzalez M, Fadeev M, Sohn YS, Nechushtai R, Willner I. Thermoplasmonic-Triggered Release of Loads from DNA-Modified Hydrogel Microcapsules Functionalized with Au Nanoparticles or Au Nanorods. Small 2020;16:e2000880.

[33] Zhang X, Feng Y, Duan S, Su L, Zhang J, He F. Mycobacterium tuberculosis strain H37Rv Electrochemical Sensor Mediated by Aptamer and AuNPs-DNA. ACS sensors 2019;4:849-55.

[34] Liu P, Wang Y, Liu Y, Tan F, Li J, Li N. S-nitrosothiols loaded mini-sized Au@silica nanorod elicits collagen depletion and mitochondrial damage in solid tumor treatment. Theranostics 2020;10:6774-89.

[35] Sargazi A, Kamali N, Shiri F, Heidari Majd M. Hyaluronic acid/polyethylene glycol nanoparticles for controlled delivery of mitoxantrone. Artificial cells, nanomedicine, and biotechnology 2018;46:500-9.

[36] Wu C, Tong Y, Wang P, Wang D, Wu S, Zhang J. Identification of impurities in methotrexate drug substances using high-performance liquid chromatography coupled with a photodiode array detector and Fourier transform ion cyclotron resonance mass spectrometry. Rapid communications in mass spectrometry : RCM 2013;27:971-8.

[37] De AK, Muthiyan R, Mondal S, Mahanta N, Bhattacharya D, Ponraj P, et al. A Natural Quinazoline Derivative from Marine Sponge Hyrtios erectus Induces Apoptosis of Breast Cancer Cells via ROS Production and Intrinsic or Extrinsic Apoptosis Pathways. Marine drugs 2019;17.

[38] Zhang Y, Hai Y, Miao Y, Qi X, Xue W, Luo Y, et al. The toxicity mechanism of different sized iron nanoparticles on human breast cancer (MCF7) cells. Food chemistry 2020;341:128263.

[39] Szoka L, Palka J. Capsaicin up-regulates pro-apoptotic activity of thiazolidinediones in glioblastoma cell line. Biomedicine & pharmacotherapy = Biomedecine & pharmacotherapie 2020;132:110741.

[40] Liu X, Ma R, Yi B, Riker A, Xi Y. MicroRNAs are involved in the development and progression of gastric cancer. Acta pharmacologica Sinica 2020.

Figures

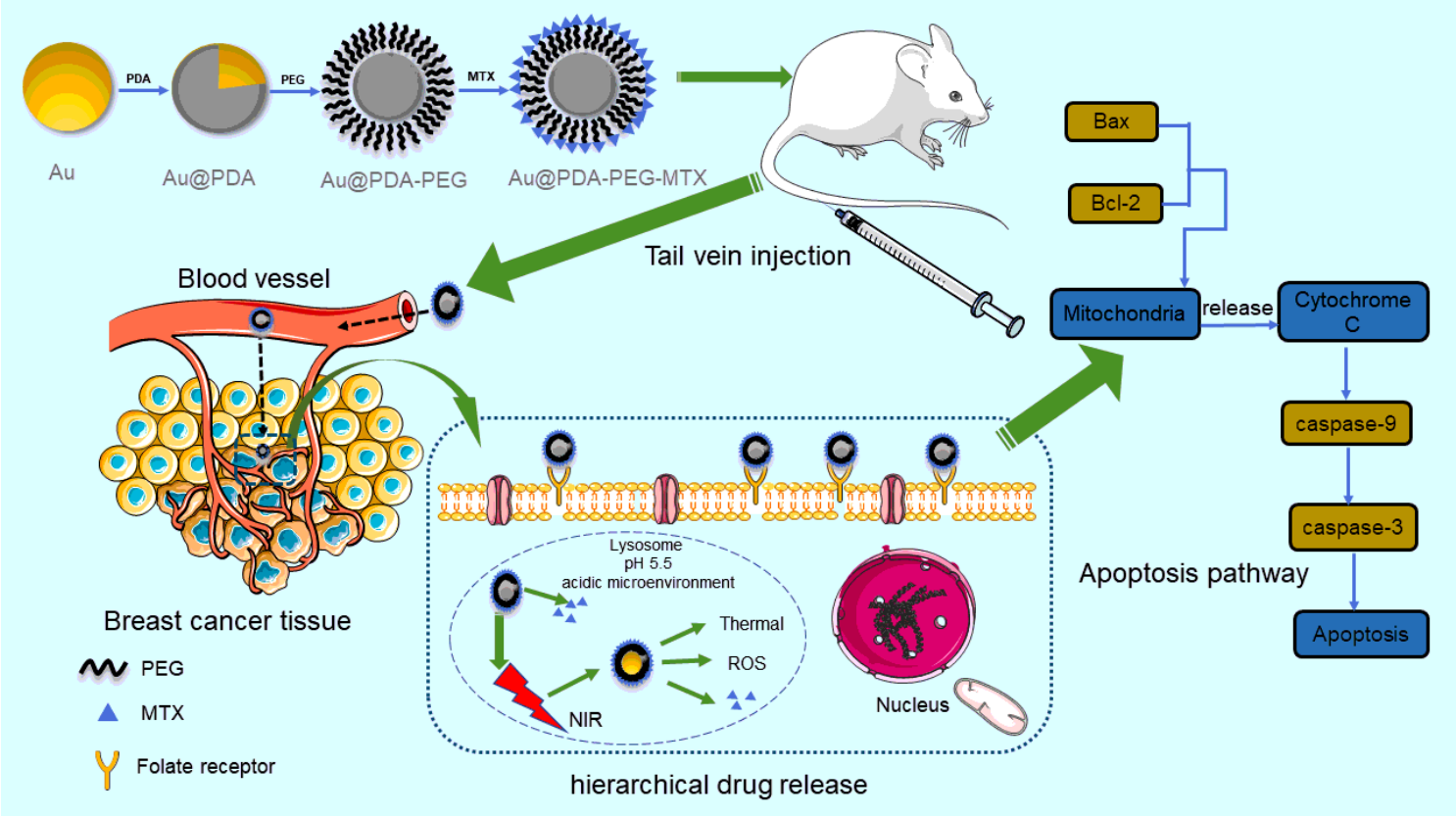

Figure 1

Process diagram for Synthesis of nanoparticles, targeting tumor tissues in vivo, releasing drugs and pathways that cause apoptosis.

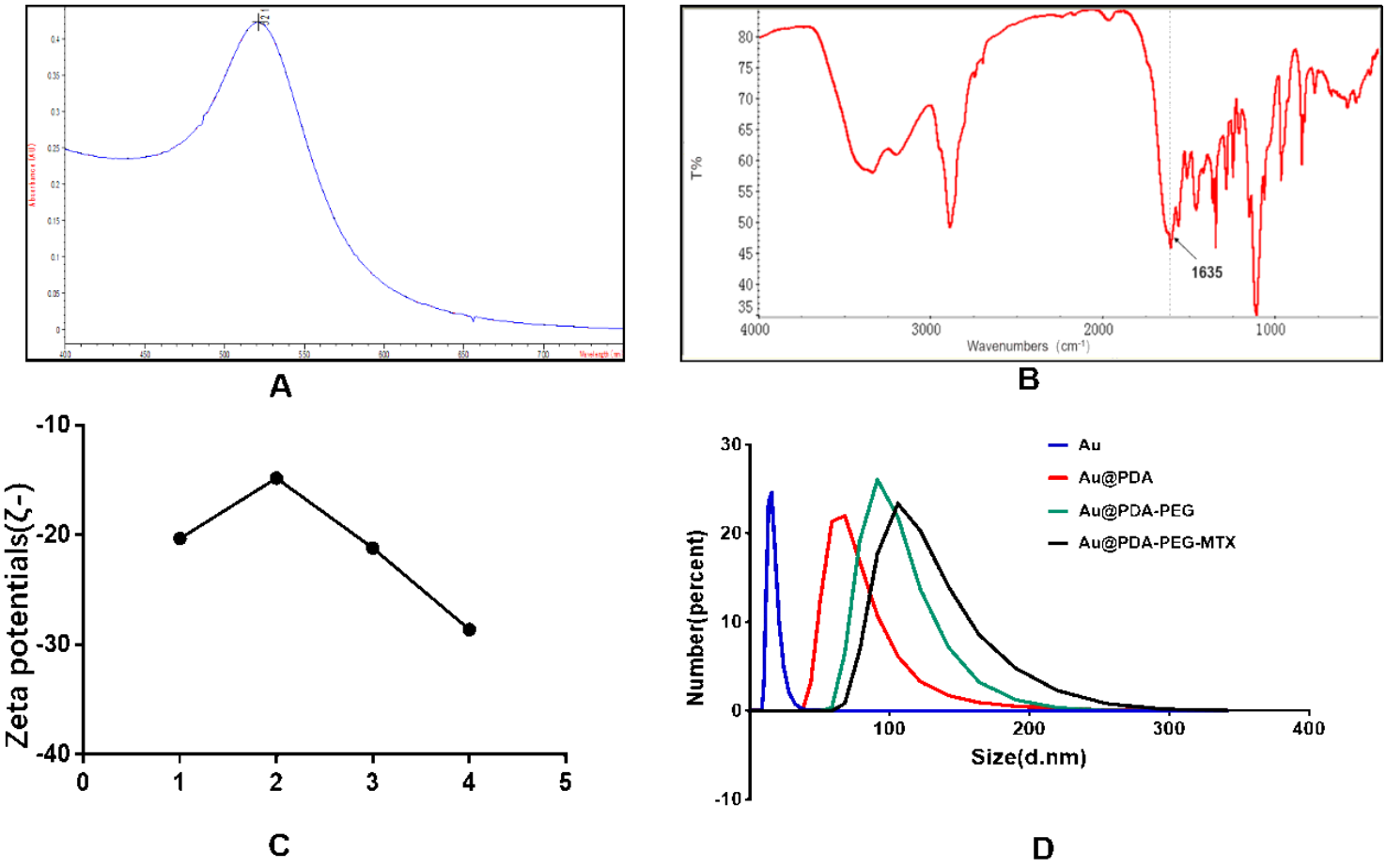

Figure 2

(A)Ultraviolet spectrum of synthesized 15nm AuNPs; (B)FT-IR spectra of the PEG-MTX; (C)Trend of Au, Au @PDA, Au @PDA-PEG-MTX zeta potential; (D) Size distribution of Au,Au @PDA,Au @PDA-PEG-MTX.

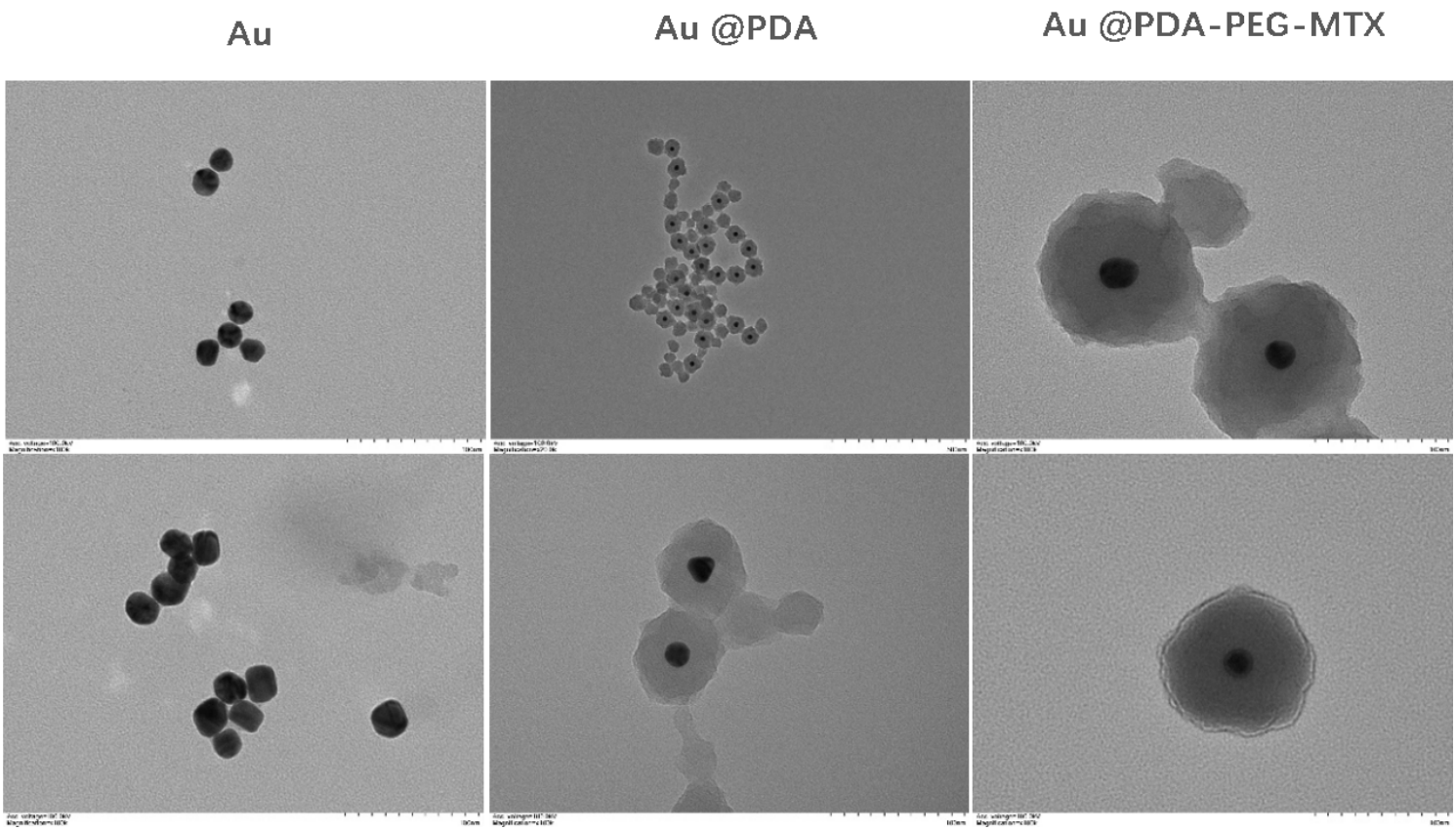

Figure 3

From left to right were the morphological characteristics of the synthesized Au, Au @PDA, Au @PDA-PEG-MTX under the TEM.

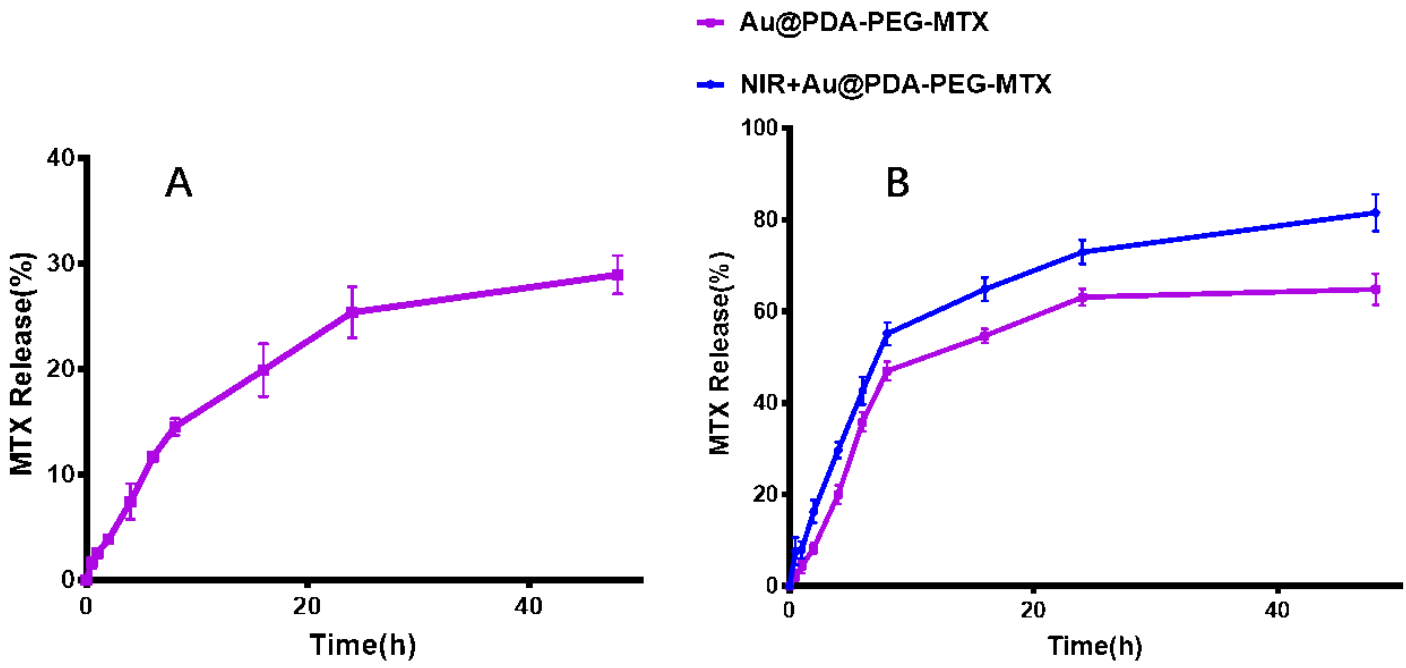

Figure 4

(A) In vitro drug release experiment, Au @PDA-PEG-MTX placed in the simulated tumor acid environment pH 5.5, MTX released by NIR irradiation with 808nm and MTX released by nanometers not irradiated by 808nm NIR; (B) Au @PDA-PEG-MTX placed in the simulated normal physiological environment pH 7.4, release of MTX by nanometers.

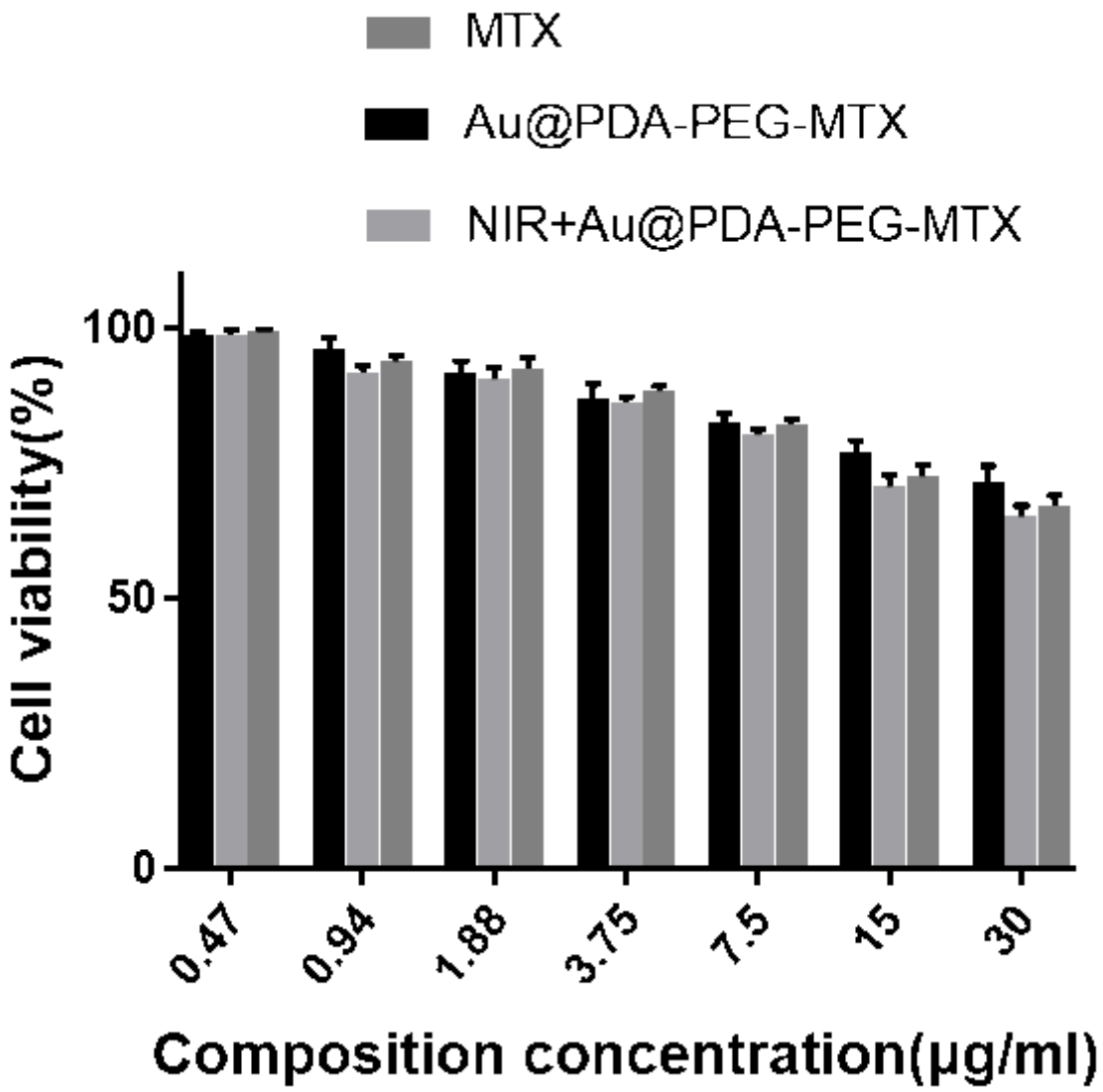

Figure 5

The cytotoxicity of MTX, Au @PDA-PEG-MTX and NIR+Au @PDA-PEG-MTX against MDA-MB-231 cells.

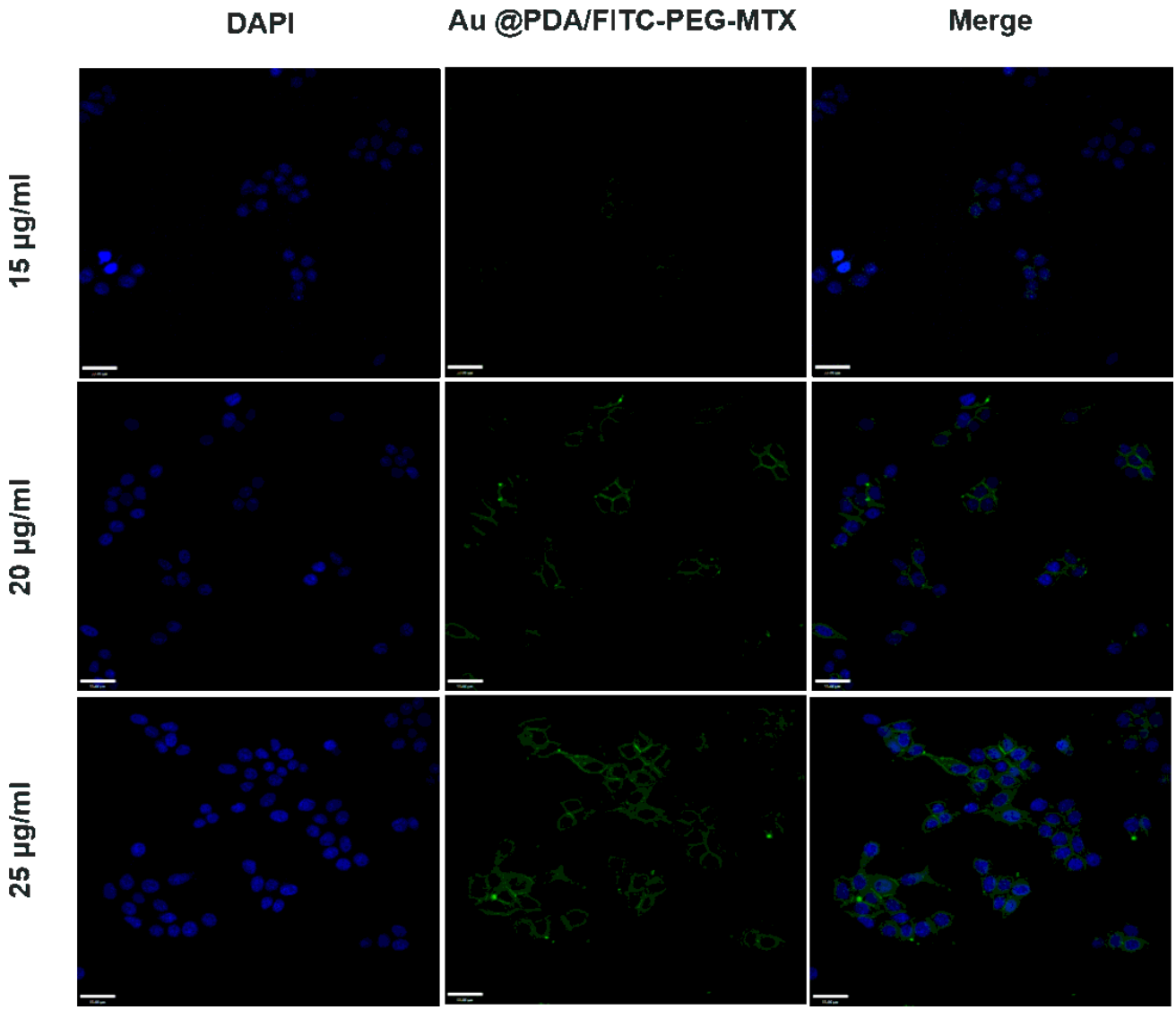

Figure 6

CLSM images of MDA-MB-231cells incubated with 15µg/ml, 20µg/ml, 25µg/ml Au @PDA-PEG-MTX.

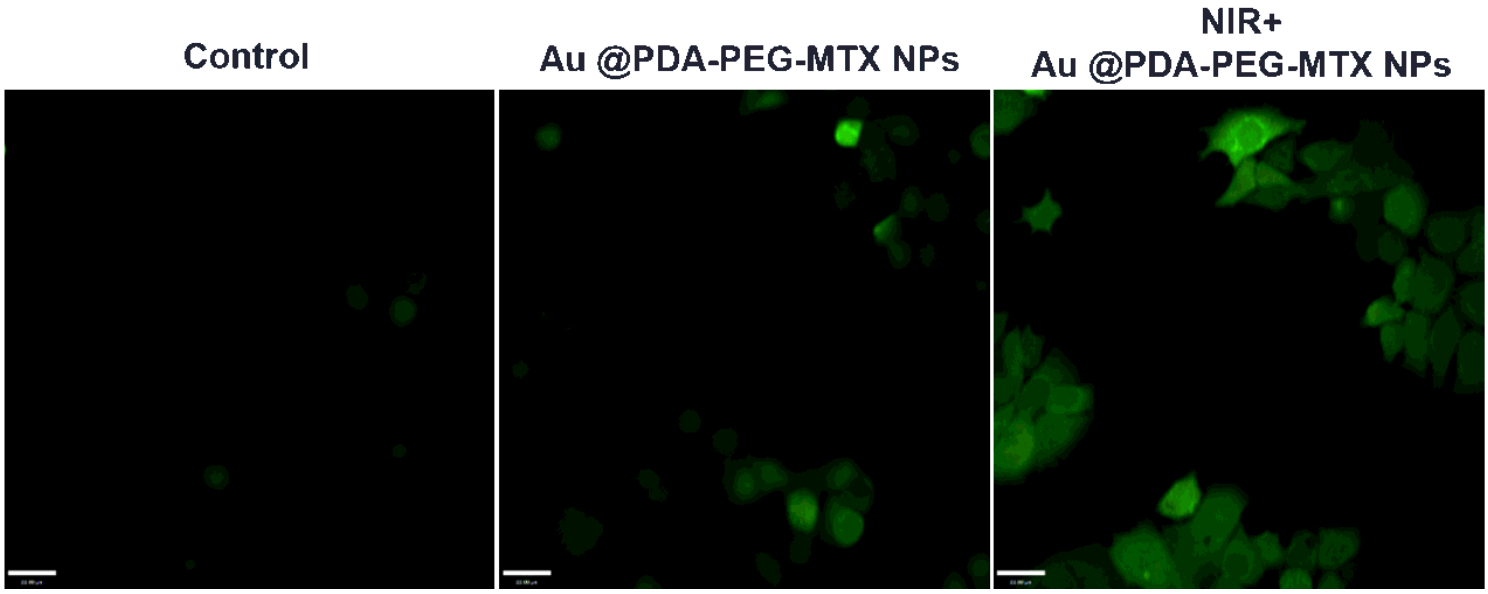

Figure 7

ROS generation in MDA-MB-231 cells with blank, Au @PDA-PEG-MTX, NIR + Au @PDA-PEG-MTX.

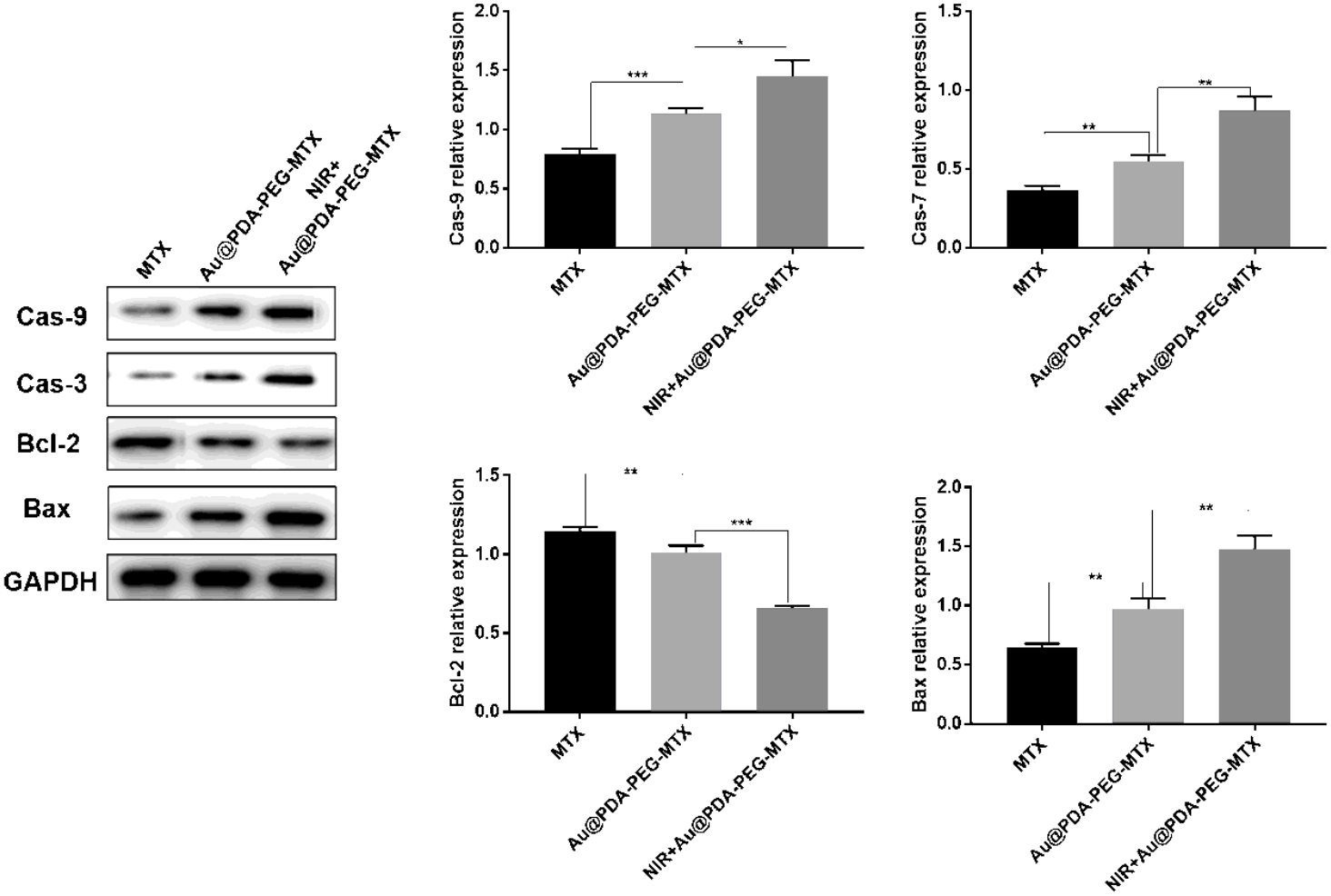

Figure 8

Expression of Cas-9, Cas-3, Bal-2, Bax protein in MTX MDA-MB-231 cells with MTX, Au @PDA-PEG-MTX and NIR+Au @PDA-PEG-MTX. *p < 0.05, **p < 0.01.

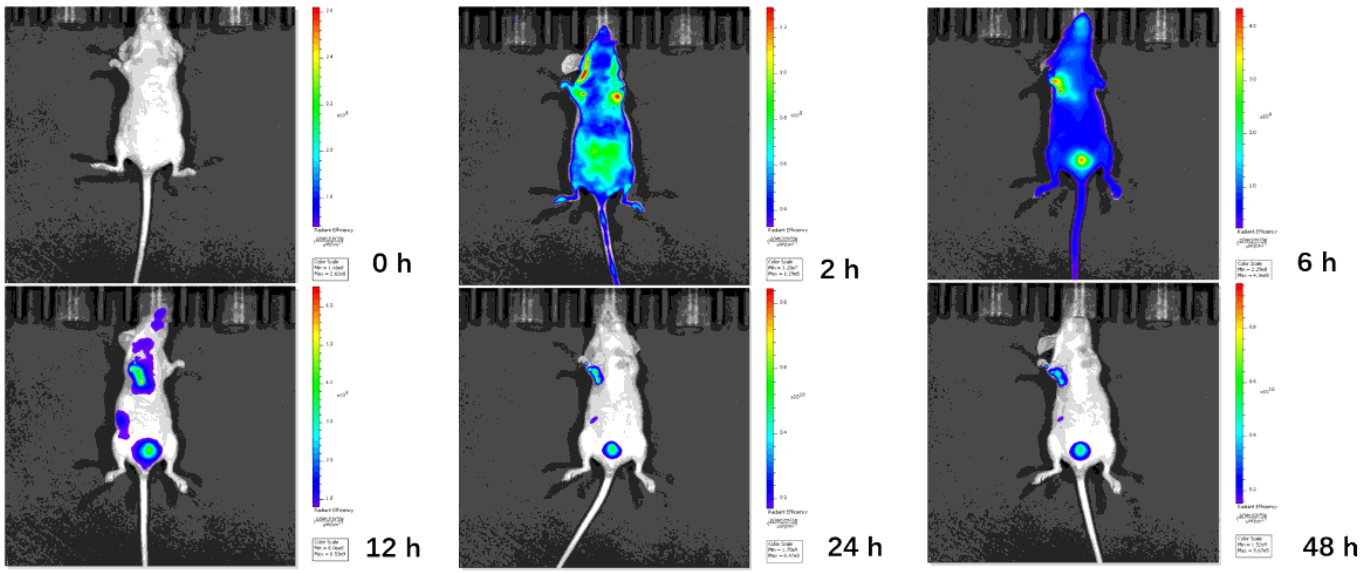

Figure 9

Real-time fluorescence imaging in vivo. In vivo bioluminescence imaging of the mice was examined at different time points.

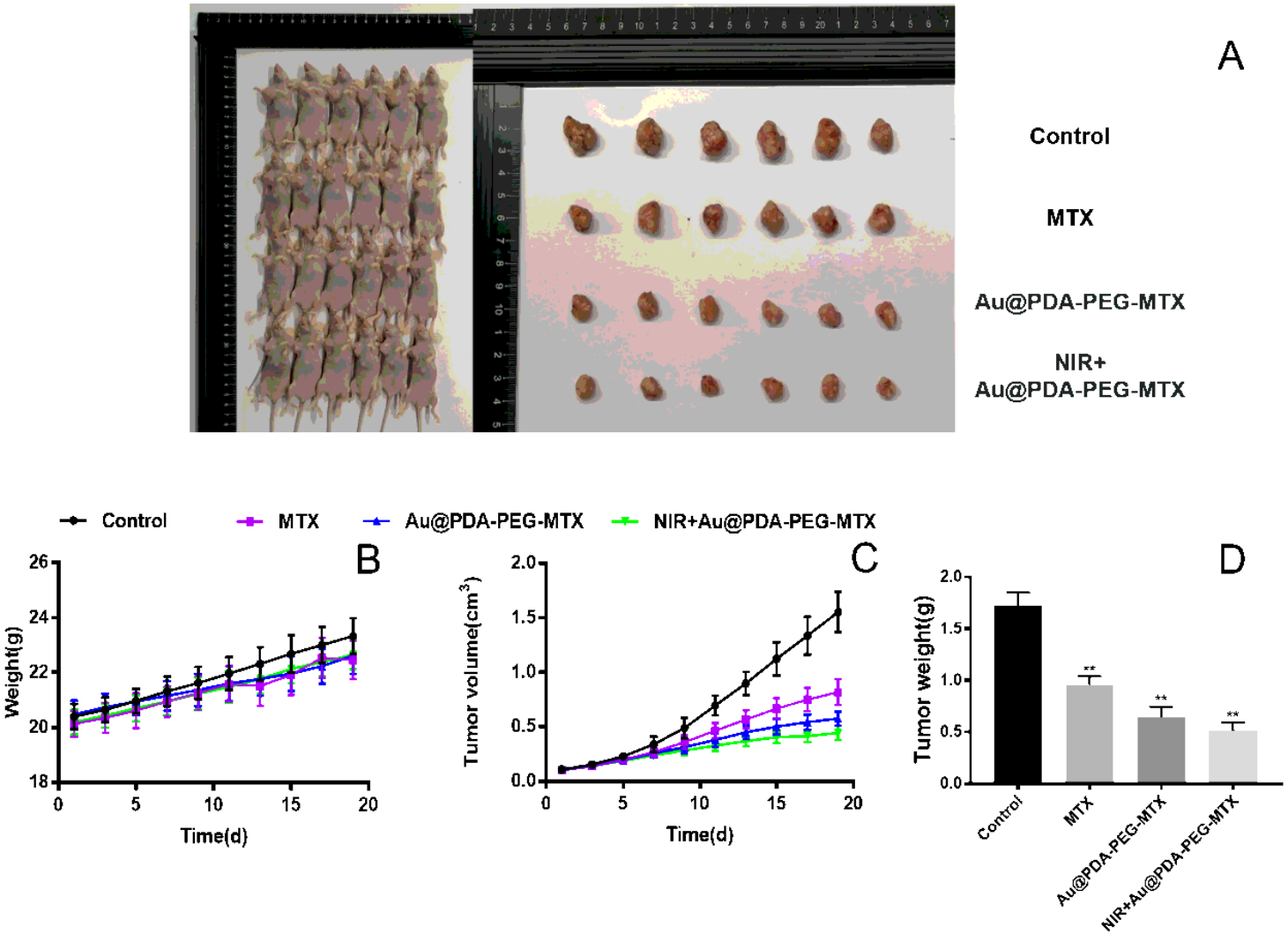

Figure 10

In vivo therapeutic effects. (A) Images of tumors; (B) Changes of BALB/c nude mice weight; (C) Changes of tumor volume; (D) Tumor weight measured in the nineteenth day. *p < 0.05, **p < 0.01.

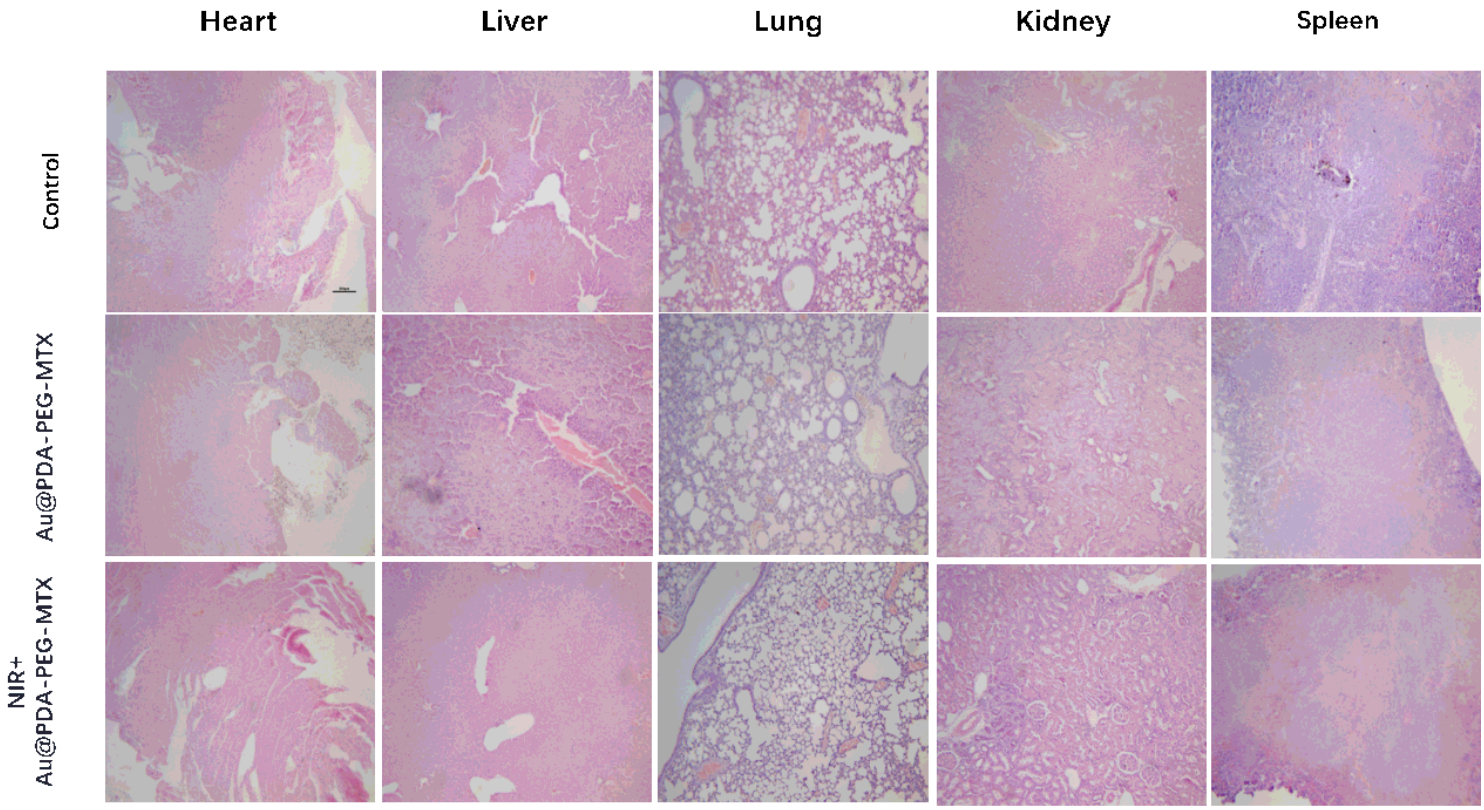

Figure 11

Histological analyses by H&E staining of heart, liver, spleen, lung, and kidney in BALB/c mice that were treated with 0.9% NaCl, Au @PDA-PEG-MTX, and NIR+Au @PDA-PEG-MTX.

Supplementary Files

This is a list of supplementary files associated with this preprint. Click to download.

- GraphicalAbstract.docx